
Unsupervised 3D Human Mesh Recovery from Noisy Point Clouds

Xinxin Zuo^{*,†} Sen Wang^{*,†} Minglun Gong[†] Li Cheng^{*}
*University of Alberta †University of Guelph
{xzuo, sen9}@ualberta.ca

Abstract

This paper presents a novel unsupervised approach to reconstruct human shape and pose from noisy point cloud. Traditional approaches search for correspondences and conduct model fitting iteratively where a good initialization is critical. Relying on large amount of dataset with ground-truth annotations, recent learning-based approaches predict correspondences for every vertice on the point cloud; Chamfer distance is usually used to minimize the distance between a deformed template model and the input point cloud. However, Chamfer distance is quite sensitive to noise and outliers, thus could be unreliable to assign correspondences. To address these issues, we model the probability distribution of the input point cloud as generated from a parametric human model under a Gaussian Mixture Model. Instead of explicitly aligning correspondences, we treat the process of correspondence search as an implicit probabilistic association by updating the posterior probability of the template model given the input. A novel unsupervised loss is further derived that penalizes the discrepancy between the deformed template and the input point cloud conditioned on the posterior probability. Our approach is very flexible, which works with both complete point cloud and incomplete ones including even a single depth image as input. Our network is trained from scratch with no need to warm-up the network with supervised data. Compared to previous unsupervised methods, our method shows the capability to deal with substantial noise and outliers. Extensive experiments conducted on various public synthetic datasets as well as a very noisy real dataset (i.e. CMU Panoptic) demonstrate the superior performance of our approach over the state-of-the-art methods. Code can be found <https://github.com/wangsen1312/unsupervised3dhuman.git>

1 Introduction

With the rapid development of sensing technology, it becomes increasingly popular to digitize human in 3D scans [11, 42]. This gives rise to a surging demand for techniques to edit, control and animate the acquired 3D content which often involves turning a 3D human scan into a SMPL model [25] or similar parametric rigged representations. Meanwhile, it is usually difficult to annotate point clouds captured in real life. This motivates us to investigate in this paper an unsupervised approach to fit a parametric rigged representation into an input human scan. Without loss of generality, we focus on fitting a SMPL model to a 3D human point cloud.

Traditional approaches address this parametric model based fitting problem using iterative closest point (ICP) strategies [2, 30]. The main idea is to iteratively search for the correspondences between the parametric model and the input scan, then re-estimate the parameters involving the pose, shape and non-rigid surface displacement of the template model. They however heavily rely on a good initialization to avoid being stuck into a local minimum solution. Existing learning based approaches [39, 23, 14], on the other hand, typically rely on well-annotated training set, being synthetic or real-world datasets. Moreover, the input point clouds are assumed to have relatively clean

surfaces. They are nonetheless difficult to deal with practical scenarios, where it is often difficult to obtain 3D shape annotations, and outliers are prevalent in the input scans. Last but not least, existing works usually requires as input the presence of a complete point cloud from full-view 3D scans. This severely limits their use when only incomplete point cloud from partial-view (e.g. a depth image) is available, a more common scenario in practice.

These observations motivate us to propose an unsupervised probabilistic-based 3D fitting approach that can cope with noisy and partial input scans. Specifically, we model the probability of the vertices on the input point cloud with a Gaussian Mixture Model (GMM) where the centroids of GMM are the vertices on the human template. In addition, we introduce a probability for the input vertices of being outliers. Basically, the network takes the point cloud as input and predicts the parameters of the template model. In the forward pass, the probabilistic correspondence association is updated as the posterior probability of the template model given the point cloud; from that we define a novel loss function which minimizes the discrepancy between the deformed template and the point cloud conditioned on the posterior probability. The network gets trained with the proposed loss function and the parameters of the template models gets updated in the backward pass of the network.

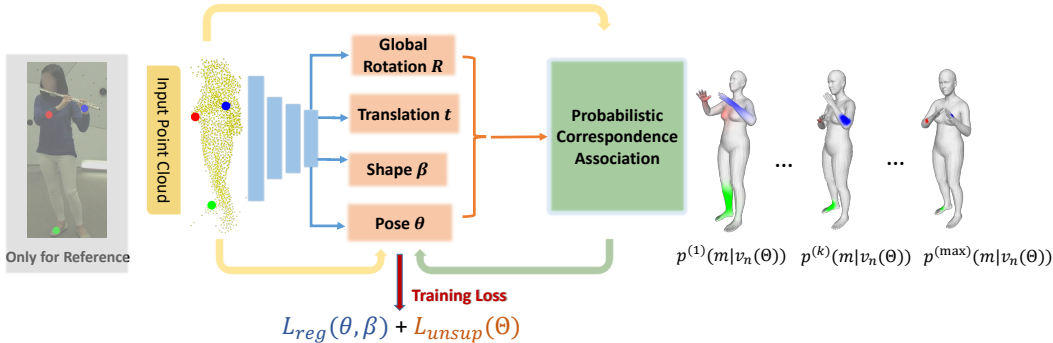


Figure 1: Overall structure. The color image is not taken as input and is shown here only for better visualization.

The overall structure is shown in Fig. 1. To illustrate the updating process, in Fig. 1 we mark three vertices over the input scan and show the updated soft correspondence association using the corresponding color over the human model. While the training proceeds, the correspondence map gets more localised and finally we get the deformed human model that fits closely to the input point cloud.

The contributions of this paper are summarized: 1) We propose a novel unsupervised method to reconstruct human shape and pose from point cloud. The network can be trained in a fully unsupervised manner with no need to warm-up the network with supervised data; 2) We propose a probabilistic loss function derived from GMM and encode the correspondences in the probability distribution which is naturally differential. It works on both complete and incomplete point cloud and is robust to outliers; 3) We evaluate the proposed method on several public datasets and outperform the current state-of-the-art methods. And we also demonstrate the effectiveness of our method in real captured noisy point cloud.

2 Related Work

2.1 Model-based Surface Fitting

Traditional approaches deal with the model fitting of 3D scans of articulated, highly non-planar objects like human bodies [6, 7] or human hands [32, 37] using nonrigid ICP based techniques [2, 30] where the correspondences matching and parametric model fitting are conducted iteratively. To account for the large pose displacement, researchers proposed to use sliding correspondences [22] or probabilistic correspondence association [41, 16] for more effective correspondence matching. However, they generally require a good model initialization, otherwise it will easily fall into local minimum. There are also approaches that focus on surface tracking [42, 30] over the 3D video sequence, in which case they usually have a predefined starting pose.

To automate the model fitting and eliminate the dependency on initialization, researchers take advantage of the deep learning techniques and train a neural network to predict the parametric model from input point cloud [21, 17, 15]. Recently, implicit functions [3, 38, 9] were proposed which is combined with the parametric model to restore the human surface details. Another branch is to predict dense correspondences between the template model and the input point cloud [4, 27], from which the parameters of the template model can be optimized. We will review the related works on correspondence matching in the following subsection. In addition to model based surface fitting, there are also efforts on general non-rigid surface registration by predicting the surface deformation [13] where the problem of topology changes would be difficult to resolve.

2.2 Correspondence

Traditional methods on shape correspondence deal with the matching problem using handcrafted local shape descriptors [1, 8, 35] which was supposed to maintain invariance under a wide class of transformations the shape can undergo. There are also efforts on finding globally consistent sets of maps [28, 19] between shapes. Operating in a low-dimension space composed of the Laplace-Beltrami basis, the Functional Maps [29] reduced dimensionality of the problem drastically by converting the point-level correspondence to the function-level correspondence.

To secure reliable correspondences, learning based methods were developed by training a neural network to predict the dense correspondences [39, 23, 14] between template model and input point cloud. For instance, targeting at human bodies, Wei [39] trained a feature descriptor on depth map pixels and treated the correspondence matching as a body region classification problem. Recently Deep Functional Maps [27, 23, 33, 14] were developed to compute correspondences across 3D shapes while optimizing for global structural properties of the surface. Another widely-used relaxation for matching problems [12, 34, 36], Optimal Transport, rely on large-scale dense matrices (e.g. geodesic distances or heat kernels) for surface matching. More recently, a self-supervised method called Loopreg [4] was proposed with a differential registration loop to predict correspondences and register template models to the input point cloud.

Although the learning based methods have been widely explored on model fitting as well as correspondence matching, they usually assume clean input point cloud and compute one-to-one correspondence. But the assumption can not hold for real captured data when the input point cloud is quite noisy with outliers. On the other hand, a large dataset with groundtruth human model annotations is also required to train the network. On the contrary, our proposed approach can work in a fully unsupervised manner and is also robust to outliers with our probabilistic correspondence association.

3 Our Approach

To reconstruct human surface from point cloud, we follow the template based surface fitting strategy. Specifically, we have the parametric human model and our goal is to optimize the parameters in the human model so that the deformed human model can match the input point cloud.

The traditional approaches solve the problem in an iterative way through correspondence search and model fitting. Mathematically, the human model is reconstructed by minimizing the following objective function

$$L(\Theta, \mathbf{c}) = \sum_{n=1}^N \text{dist}(\mathbf{v}_n, M(\mathbf{c}_m, \Theta)), \quad (1)$$

where \mathbf{c}_m denotes the correspondences in the human model for \mathbf{v}_n from input point cloud which are usually computed via nearest search, and the human model ($M(\Theta)$) gets updated by minimizing the distance function $\text{dist}(\cdot)$ which can be point-to-point or point-to-surface distance between the correspondences. However, the optimization will fall into local minimal especially when the initial model is far away from the input.

Generally, the above distance metrics or Chamfer loss are also used as an unsupervised loss to train the network for model registration [4, 21]. However, similar to the local minimal in traditional model fitting approaches, it is hard for the network to converge if trained with the above distance loss without using supervised data to warm-up the network. In addition, this distance function is sensitive to outliers. When we consider the correspondence association, it is not appropriate to

assign correspondences for vertices belonging to outliers, where the previous methods usually predict correspondences for every vertex of the input point cloud.

In this paper, instead of explicitly assigning correspondences, we propose a probabilistic correspondence association module and define a novel distance function as the unsupervised fitting loss which can be differential and robust to outliers. The proposed loss function allows us to train the network from scratch. Next, we will describe the derivation of our loss function in detail.

Mixture Model. Our loss function builds upon the GMM where the input point cloud are assumed to be generated by a GMM whose centroids are the vertices of the deformed template model. To further compensate for the outliers in the input point cloud, we use a uniform distribution to define the probability of the vertices being outliers. Mathematically, the probability of each vertex of the input scan \mathbf{v}_n can be expressed as

$$p(\mathbf{v}_n) = (1 - \mu) \sum_{m=1}^M p(m)p(\mathbf{v}_n|m) + \mu \frac{1}{N} = (1 - \mu) \sum_{m=1}^M \pi_{mn} \mathcal{N}(\mathbf{v}_n|m) + \mu \frac{1}{N}, \quad (2)$$

where N and M are the number of vertices of the input point cloud and the template human model respectively. $\mathcal{N}(\mathbf{v}_n|m)$ is a normal distribution and μ is the approximation for the percentage of outliers, which is considered to be evenly distributed. π_{mn} represents the coefficients of the mixture model which can be viewed as the probability of assigning vertice \mathbf{v}_n in the input point cloud and the vertice M_m on the human model as correspondence.

We use equal isotropic covariances σ^2 for the Gaussian model and therefore the conditional distribution $p(\mathbf{v}_n|m)$ is formulated as

$$p(\mathbf{v}_n|m) = \frac{1}{(2\pi\sigma^2)^{\frac{3}{2}}} \exp\left(-\frac{\|M_m(\Theta) - \mathbf{v}_n\|^2}{2\sigma^2}\right). \quad (3)$$

In the above conditioned probability function, $M(\Theta)$ is the parametric human model of the parameters $\Theta = \{\theta, \beta, R, t\}$. The proposed techniques can apply generally to any 3D statistical model and in this paper, we have used the SMPL human model which is parameterized by the shape β and pose θ coefficients. R and t are the global rotation matrix and translation vector to transform the human model to the input point cloud. More details about the SMPL model can be found in paper [25].

Under the i.i.d assumption, the energy function is defined as minimizing the negative log-likelihood for all the vertices

$$E(\Theta, \sigma^2) = - \sum_{n=1}^N \log \left((1 - \mu) \sum_{m=1}^M \pi_{mn} \frac{1}{(2\pi\sigma^2)^{\frac{3}{2}}} \exp\left(-\frac{\|M_m(\Theta) - \mathbf{v}_n\|^2}{2\sigma^2}\right) + \mu \frac{1}{N} \right). \quad (4)$$

Inspired by EM based optimization procedure to solve the above energy function iteratively [10], we design the network with a probability association module in the forward pass to update the posterior distribution $p(m|\mathbf{v}_n)$ and resolve the human model parameters in the backward training.

Probabilistic Correspondence Association. Similar to the E-step of the EM optimization, given the parameters predicted by the network from the previous iteration, we update the posterior distribution of the vertices on the human model conditioned on the input point cloud by

$$p^{(k)}(m|\mathbf{v}_n(\Theta)) = \frac{\exp\left(-\frac{\|\mathbf{v}_n - M_m(\Theta^{(k-1)})\|^2}{2\sigma_{k-1}^2}\right)}{\sum_{i=1}^M \exp\left(-\frac{\|\mathbf{v}_n - M_i(\Theta^{(k-1)})\|^2}{2\sigma_{k-1}^2}\right) + c}, \quad (5)$$

where $c = (2\pi(\sigma_{k-1})^2)^{\frac{3}{2}} \frac{1-\mu}{\mu} \frac{M}{N}$, and k denotes the training iteration. In our current scenario, the posterior distribution computation corresponds to the correspondence matching between the template model and the input point cloud. Compared with LoopReg [4] which uses a diffusion field to differentiate the correspondence matching operation, our probabilistic correspondences association is naturally differential without including extra effort.

Unsupervised Loss. Taking the computed posterior distribution into Eq. 4, we can then update the human model parameters Θ by minimizing the following complete negative log-likelihood function.

$$Q(\Theta, \sigma^2) = \frac{1}{2\sigma^2} \sum_{n,m=1}^{N,M} p^{(k)}(m|\mathbf{v}_n(\Theta)) \|\mathbf{v}_n - M_m(\Theta)\|^2 + \frac{3}{2} N_P \log \sigma^2, \quad (6)$$

$$N_P = \sum_{n=1}^N \sum_{m=1}^M p^{(k)}(m|\mathbf{v}_n(\Theta)). \quad (7)$$

In the above function (Eq. 6), for the typical EM optimization process, Θ and σ^2 are supposed to be updated in the M-step. In our case, taking the point cloud as input, the network predicts the parameters Θ of the human model. But σ is not controlled directly by the input point cloud, instead, it is treated as a hyper-parameter in the loss function. We develop a strategy to update σ during the training iteration. Therefore, neglecting the second term in Eq. 6 which has no dependency with respect to the model parameters, we define our unsupervised loss function as

$$L_{unsup}(\Theta) = \frac{1}{2\sigma^2} \sum_{n,m=1}^{N,M} p^{(k)}(m|\mathbf{v}_n(\Theta)) \|\mathbf{v}_n - M_m(\Theta)\|^2. \quad (8)$$

To prevent arbitrary poses and shapes, our training loss also include three regularization terms for the predicted human shape and pose parameters [5, 20],

$$L_{reg}(\theta, \beta) = \lambda_\theta L_\theta(\theta) + \lambda_a L_a(\theta) + \lambda_\beta L_\beta(\beta), \quad (9)$$

where $L_\theta(\theta)$ is a mixture of Gaussian pose prior trained with shapes fitted on marker data [24], $L_a(\theta)$ is a pose prior penalizing unnatural rotations of elbows and knees, while $L_\beta(\beta)$ is a quadratic penalty on the shape coefficients.

Finally, the overall loss function to train the network is expressed as

$$L = L_{unsup}(\Theta) + L_{reg}(\theta, \beta). \quad (10)$$

Update of σ^2 . In Eq. 3, the hyper-parameter σ^2 represents the variance of the Gaussian distribution controlling the certainty of the matching between the human model and input point cloud. Therefore, in the early iterations σ is supposed to be larger since the initial human model has large distance to the input point cloud and we have great matching uncertainty. σ gets smaller as the iteration proceeds. When $\sigma \rightarrow 0$, the posterior distribution (Eq. 5) will be close to a one-hot vector and our proposed loss function will approximate the classical Chamfer distance. In this way, we can see our proposed loss function as a generalized Chamfer distance with soft correspondences.

In the typical EM optimization process, σ^2 is updated via the following equation (Eq. 11), which is derived by setting the derivatives of $Q(\Theta, \sigma^2)$ to zero with respect to σ^2 ,

$$\sigma^2 = \frac{1}{3N_P} \sum_{n=1}^N \sum_{m=1}^M p^{(k)}(m|\mathbf{v}_n(\Theta)) \|\mathbf{v}_n - M_m(\Theta)\|^2. \quad (11)$$

As shown in the above equation, the update of σ^2 relies on the posterior probability of previous iteration which requires extra efforts to memorize and maintain it. In addition, different from traditional EM optimization, σ^2 will also get affected by the current status of the network. Therefore, we re-compute the posterior probability matrix with a σ_{itr} decreasing along with the training epoch and then update the current σ^2 via Eq. 11.

Global Pose Estimation. Our network predicts the human model parameters which include shape, local pose and global pose parameters. For global pose estimation, it is hard to train a neural network to directly predict the rotation matrix $\mathbf{R} \in \mathbb{R}^{3 \times 3}$. Instead of using Euler angles to represent the global rotation [3, 4], in this paper we employ the 6D rotation representation which has been proved to be continuous in real Euclidean spaces and more suitable for learning [43, 40]. Mathematically, we use the vector $\mathbf{b} = (\mathbf{b}_x, \mathbf{b}_y) \in \mathbb{R}^6$, $\mathbf{b}_x \in \mathbb{R}^3$, $\mathbf{b}_y \in \mathbb{R}^3$ to present the rotation, from which the rotation matrix $\mathbf{R} = (\mathbf{R}_x, \mathbf{R}_y, \mathbf{R}_z)^T \in \mathbb{R}^{3 \times 3}$ can be obtained by

$$\mathbf{R}_x = N(\mathbf{b}_x), \quad \mathbf{R}_z = N(\mathbf{R}_x \times \mathbf{b}_y), \quad \mathbf{R}_y = \mathbf{R}_z \times \mathbf{R}_x, \quad (12)$$

where $\mathbf{R}_x, \mathbf{R}_y, \mathbf{R}_z \in \mathbb{R}^3$, N is a normalization function, " \times " means cross product.

In the experimental section, we validate the effectiveness of using 6D representation in our framework.

Network Structure. Our network takes the point cloud as input and we use PointNet++ [31] to regress the parameters of the SMPL model. The network is trained from scratch and in the forward

pass the probabilistic correspondences association is updated by computing the posterior distribution of the input point cloud given the current predicted human model, and the network is trained with our proposed unsupervised loss to update the human model parameters via back-propagation.

Compatible with Complete and Incomplete Point Clouds. Previous methods on unsupervised human reconstruction or correspondence matching are usually designed to work with relatively complete point cloud [4, 38, 21]. To deal with in-complete point cloud, especially for the point cloud acquired from depth map where a great portion of the data is invisible, the existing works always rely on large human dataset with strong supervision [3]. To be different, our proposed unsupervised method can naturally work with incomplete point cloud and the success comes from our implicit correspondence association in which we do not need to predict one-to-one correspondence between the template model and the input point cloud. We demonstrate the effectiveness of our method on human shape and pose reconstruction from a depth map in the experiments.

Implementation details. Our network takes a point cloud of 2048 vertices as input which is sampled from the 3D human scans with farthest point sampling. In our loss function(Eq. 9), λ_θ , λ_a and λ_β is set as 20.0, 225.0 and 25.0 respectively. σ_{itr}^2 is initialized as 0.1. We further improve the reconstruction with an instance-level optimization. Specifically, starting from the parametric model predicted from our network, we minimize the objective function defined in Eq. 3 with EM optimization.

4 Experiments

4.1 Datasets

In this paper, we have considered three public datasets on human modeling: CAPE, FAUST and CMU Panoptic PointCloud Dataset.

The CAPE dataset [26] provides 148,584 pairs of scans under clothing and registered ground truth body shapes for 15 subjects of different genders. The FAUST dataset [6] consists of 100 training and 200 testing scans. They may include noise and have holes, typically missing part of the feet. In this paper, we have not used the training set to train our network, instead we only evaluated the correspondence matching results on the test set and made comparison with other methods. The CMU Panoptic PointCloud Dataset [18] is captured by 10 Synchronized Kinects. Compared with other 3D point cloud datasets, the captured human surface is quite noisy and contains large amount of vertices which do not belong to the human surface. For example, there are sequences of human subject playing musical instruments. Among the captured sequences, we choose the sequences containing single human subject that have ground-truth 3D joints for testing.

Training Set. We have split the CAPE dataset into training and testing set. Specifically, we use 12 subjects for training and 3 subjects for testing. We also subsampled the recordings by a factor of 5. The final training set consists of 26,004 frames while the validation set consists of 3,965 frames. We generated input point clouds by sampling 2,048 points on the surfaces of the clothed meshes and add Gaussian noise of zero mean and 1mm standard-deviation. In this paper our network was trained on the CAPE training set but evaluated directly on other datasets without further fine-tuning.

4.2 Comparisons on Human Shape and Pose Reconstruction

Comparison Methods. We compared with three state-of-the-art methods on human model reconstruction from point cloud, namely 3D-CODED [15], IPNet [3] and PTF [38], all of which are supervised approaches trained with groundtruth annotation. Both IPNet and PTF exploited implicit representations and SMPL based parametric model for surface fitting. 3D-CODED also adopted the SMPL template and directly regressed the deformation and predicted the deformed template model. For fair comparison, we compute the error of the predicted SMPL model. Besides, the 3D-CODED method cannot apply on the point cloud since they require a 3D mesh as input. Therefore, 3D-CODED method was not evaluated on CMU Panoptic PointCloud Dataset.

4.2.1 Evaluation on CAPE Dataset

Evaluation Metrics. First, the vertex-to-vertex (V2V) error is computed as the distance between the vertex on the predicted SMPL model and the corresponding vertex on the groundtruth. Besides, we also report Chamfer distance (CD) which is a common evaluation indicator for surface registration.

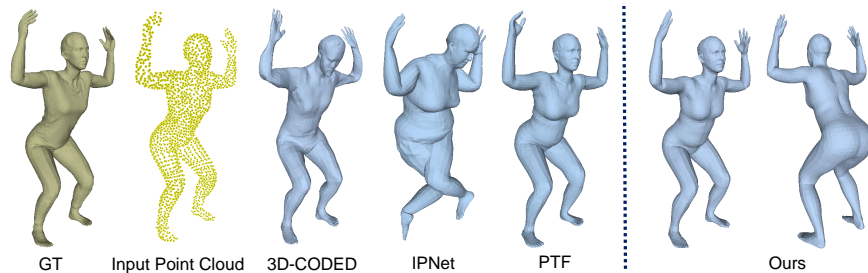


Figure 2: Qualitative evaluation on CAPE. From left to right, we show the ground-truth clothed meshes [26], input point clouds, SMPL meshes reconstructed by 3D-CODED [15], IPNet [3], PTF [38] and our results from different views.

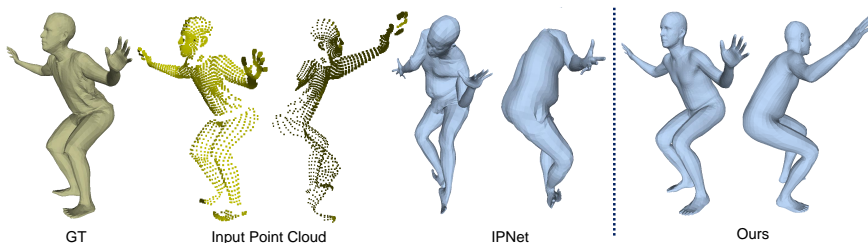


Figure 3: Qualitative evaluation on CAPE of incomplete data. From left to right, we show the ground-truth clothed meshes [26], input point clouds, SMPL meshes reconstructed by IPNet [3], and ours from different views.

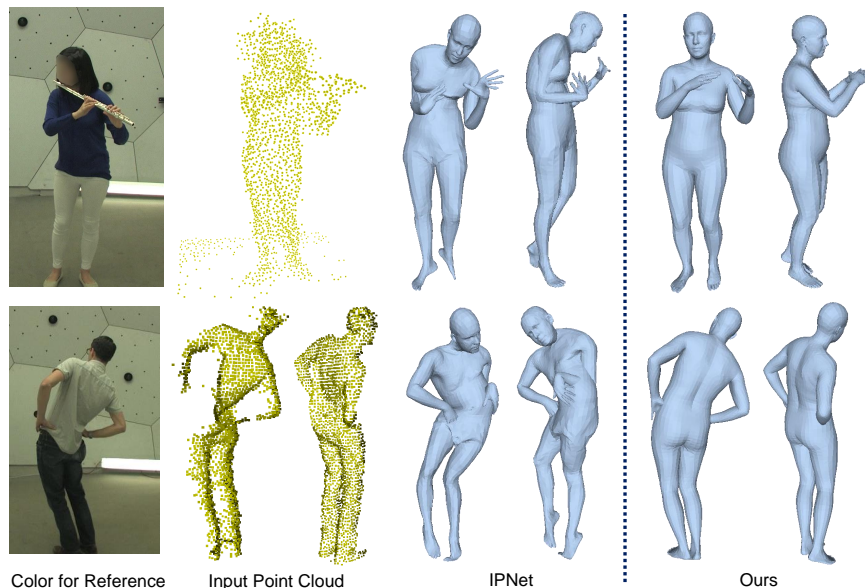


Figure 4: Qualitative evaluation on CMU Panoptic. From left to right, we show the reference color image, input point clouds, SMPL mesh reconstructed by IPNet [3] and ours from different views. The color image is not used as input but only for visualization purpose.

In Tab. 1, we demonstrate the evaluation results of 3D-CODED, IPNet, PTF and ours. For IPNet and 3D-CODED approaches, we use the trained network released by the authors. On the other hand, since we share the same training and testing set split with PTF, so we refer to their paper for the evaluated results. To validate the effectiveness of our method for incomplete point cloud. We have generated depth maps for the models in CAPE dataset by rendering the human mesh into randomly generated camera coordinates rotating around the human subject. As shown in Tab. 1, our proposed methods

Method	Point Cloud		Depth	
	V2V(mm)	CD(mm)	V2V(mm)	CD(mm)
3D-CODED [15]	35.7	20.4	-	-
PTF [38]	23.1	14.8	-	-
IPNet [3]	28.2	15.1	60.2	47.2
Ours	21.8	13.2	48.6	33.2

Table 1: Quantitative evaluation on CAPE dataset.

even outperforms the existing supervised approaches with smallest V2V and CD error for both complete point cloud and incomplete point cloud indicated as Depth. Since PTF and 3D-CODED cannot directly extend to incomplete point cloud, the corresponding error is not reported in the table. In addition to quantitative evaluation, we also visualize some sampled results in Fig. 2 and Fig. 3. More visualization results can be found in the supplementary.

4.2.2 Evaluation on CMU Panoptic Dataset

Evaluation Metrics. For the CMU Panoptic dataset, we do not have the groundtruth SMPL for the captured point cloud. Instead, the groundtruth 3D joints are provided. Therefore, we use Mean Per Joint Position Error (MPJPE) as evaluation protocol which is computed as the average Euclidean distance of predicted joints to the ground-truth. In addition, percent of correct keypoints (PCK) error is also reported where computed joint is considered correct if its distance to the groundtruth is within a certain threshold (100 mm in this paper).

In Tab. 2, we show the error of joints extracted from the predicted SMPL model and also report the error on both complete and incomplete point cloud. For the complete point cloud we used the point cloud merged from all the 10 Kinects and for incomplete point cloud we used the depth map randomly selected from those Kinects. As shown in Tab. 2, the proposed method has achieved better performance with smaller error for both MPJPE and PCK. Some sampled results are displayed in Fig. 4, from which we can that the proposed method is robust to noisy input point cloud that have great outliers. More visualization results can be found in the supplementary.

Method	Point Cloud		Depth	
	MPJPE (mm)↓	PCK↑	MPJPE (mm)↓	PCK↑
IPNet [3]	43.8	73.2	56.8	57.2
Ours	25.7	89.6	37.6	79.2

Table 2: Joints error on CMU Panoptic dataset.

4.3 Comparison on Correspondence Prediction

Comparison Methods. We have compared with several existing approaches on correspondence matching. Specifically, FMNet [23] and LoopReg [4] can directly regress the correspondences while 3D-CODED [15], LBS-AE [21] as well as our proposed approach use the predicted template model as the bridge to compute the correspondences between different scans. Among those methods, FMNet and 3D-CODED are supervised approaches while LoopReg and LBS-AE are unsupervised ones, but they still rely on supervised data to warm-up the training.

Evaluation on FAUST Dataset. We have compared with previous approaches of correspondence matching on FAUST dataset [6] with the results shown in Tab. 3. We follow the evaluation metric in paper [4] and report the correspondence error as Euclidean distance of the predicted correspondence to the groundtruth for both Inter-class and Intra-class. As shown in Tab. 3, our proposed method has

Metrics	FMNet [23]	LBS-AE [21]	3D-CODED [15]	LoopReg [4]	Ours
Inter-class (mm)	48.3	40.8	28.7	26.6	22.38
Intra-class (mm)	24.4	21.6	19.8	13.4	9.97

Table 3: Correspondence evaluation on FAUST dataset. Our method clearly outperforms the state-of-the-art supervised [23, 15] and unsupervised [21, 4] approaches.

achieved the best performance on both cases and the matching error was reduced in a large margin especially for the Intra-class scenario.

4.4 Ablation Study

In this section, we conducted ablation studies on several key components of the proposed method. We implemented the following ablation studies on the CAPE dataset.

Robustness to Noise. We have added both Gaussian noise and random outliers for the models in the CAPE test set. In Tab. 4, we can see that while increasing the standard deviation of the Gaussian noise and the percentage of random outliers, compared with IPNet [3] that has not considered the noise, the V2V and Chamfer errors of the predicted human surface from our proposed method had a rather small increase. For example, after adding Gaussian noise with 5mm standard deviation and 5% percentage of outliers, the V2V and Chamfer errors of our predicted human model only increased by 1.1mm and 1.3mm respectively. On the contrary, the errors of IPNet have increased greatly.

Noise	Standard Deviation (mm)				
	0	5	10	20	50
	Outlier Percentage				
	0%	5%	10%	15%	20%
IPNet [3] V2V(mm)	28.2	57.4	62.3	67.5	73.8
IPNet [3] CD(mm)	15.1	31.8	33.2	38.4	40.2
ours V2V(mm)	21.8	22.9	26.7	28.2	32.5
ours CD(mm)	13.2	14.5	15.8	16.7	19.2

Table 4: Ablation study on surface noise.

6D Pose Estimation. In Tab. 5, we demonstrate the effectiveness of using 6D representation in pose estimation. As compared with the widely used Euler angle or axis-angle representation, we have achieved better results with smaller surface error on the reconstructed human model using 6D representation [43].

Method	Point Cloud		Depth	
	V2V(mm)	CD(mm)	V2V(mm)	CD(mm)
Ours without 6D vector	26.1	14.7	57.2	38.9
Ours with 6D vector	21.8	13.2	48.6	33.2

Table 5: Ablation study on 6D pose representation.

Update of σ^2 . In Fig. 5, we show sampled comparison results of the reconstructed human model w/o updating σ^2 during training. Trained with small σ^2 , the network will have similar performance as using Chamfer distance where it is difficult for the training to converge. On the other hand, as demonstrated in Fig. 5, with large σ^2 the network lacks the ability to precisely fit to the input scan. On the contrary, with our proposed updating strategy, we can have better fitting to the input point cloud.

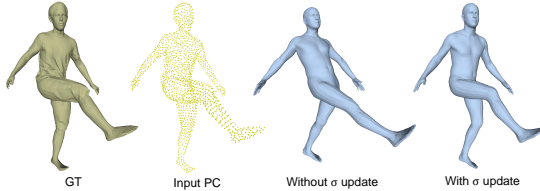


Figure 5: Ablation study on σ^2

5 Conclusion

In this paper, a novel unsupervised approach was proposed to reconstruct human shape and pose from an input point cloud. Instead of explicitly predicting or regressing the correspondences for each vertice of the point cloud, which has no tolerance to outliers, we have adopted GMM to model the input point cloud and implicitly encoded the correspondences with probabilistic association. A novel loss function was proposed to train the network from scratch in a fully unsupervised manner, which is also robust to a significant amount of outliers. We have conducted evaluation on several public datasets and outperformed both supervised and unsupervised state-of-the-art methods. As a limitation, we have not explicitly addressed the collision problem in this paper which makes it difficult to precisely reconstruct the human surface when the human body has close self-interaction. As a future work, we could include body part information to resolve this issue.

References

- [1] M. Aubry, U. Schlickewei, and D. Cremers. The wave kernel signature: A quantum mechanical approach to shape analysis. In *2011 IEEE international conference on computer vision workshops (ICCV workshops)*, pages 1626–1633. IEEE, 2011.
- [2] P. J. Besl and N. D. McKay. Method for registration of 3-d shapes. *IEEE Transactions on Pattern Analysis and Machine Intelligence*, 14(2):586–606, 1992.
- [3] B. L. Bhatnagar, C. Sminchisescu, C. Theobalt, and G. Pons-Moll. Combining implicit function learning and parametric models for 3d human reconstruction. In *Proceedings of the European Conference on Computer Vision (ECCV)*, pages 311–329, 2020.
- [4] B. L. Bhatnagar, C. Sminchisescu, C. Theobalt, and G. Pons-Moll. Loopreg: Self-supervised learning of implicit surface correspondences, pose and shape for 3d human mesh registration. In *Advances in neural information processing systems*, pages 12909–12922, 2020.
- [5] F. Bogo, A. Kanazawa, C. Lassner, P. Gehler, J. Romero, and M. J. Black. Keep it smpl: Automatic estimation of 3d human pose and shape from a single image. In *European conference on Computer Vision (ECCV)*, pages 561–578. Springer, 2016.
- [6] F. Bogo, J. Romero, M. Loper, and M. J. Black. FAUST: Dataset and evaluation for 3D mesh registration. In *Proceedings of the IEEE Conference on Computer Vision and Pattern Recognition*, pages 3794–3801, 2014.
- [7] F. Bogo, J. Romero, G. Pons-Moll, and M. J. Black. Dynamic faust: Registering human bodies in motion. In *Proceedings of the IEEE conference on computer vision and pattern recognition*, pages 6233–6242, 2017.
- [8] M. M. Bronstein and I. Kokkinos. Scale-invariant heat kernel signatures for non-rigid shape recognition. In *2010 IEEE Computer Society Conference on Computer Vision and Pattern Recognition*, pages 1704–1711. IEEE, 2010.
- [9] J. Chibane, T. Alldieck, and G. Pons-Moll. Implicit functions in feature space for 3d shape reconstruction and completion. In *Proceedings of the IEEE/CVF Conference on Computer Vision and Pattern Recognition*, pages 6970–6981, 2020.
- [10] A. P. Dempster, N. M. Laird, and D. B. Rubin. Maximum likelihood from incomplete data via the em algorithm. *Journal of the Royal Statistical Society: Series B (Methodological)*, 39(1):1–22, 1977.
- [11] M. Dou, S. Khamis, Y. Degtyarev, P. Davidson, S. R. Fanello, A. Kowdle, S. O. Escolano, C. Rhemann, D. Kim, J. Taylor, et al. Fusion4d: Real-time performance capture of challenging scenes. *ACM Transactions on Graphics (ToG)*, 35(4):1–13, 2016.
- [12] M. Eisenberger, A. Toker, L. Leal-Taixé, and D. Cremers. Deep shells: Unsupervised shape correspondence with optimal transport. *arXiv preprint arXiv:2010.15261*, 2020.
- [13] W. Feng, J. Zhang, H. Cai, H. Xu, J. Hou, and H. Bao. Recurrent multi-view alignment network for unsupervised surface registration. In *Proceedings of the IEEE/CVF Conference on Computer Vision and Pattern Recognition*, pages 10297–10307, 2021.
- [14] D. Ginzburg and D. Raviv. Cyclic functional mapping: Self-supervised correspondence between non-isometric deformable shapes. In *European Conference on Computer Vision*, pages 36–52. Springer, 2020.
- [15] T. Groueix, M. Fisher, V. G. Kim, B. C. Russell, and M. Aubry. 3d-coded: 3d correspondences by deep deformation. In *Proceedings of the European Conference on Computer Vision (ECCV)*, pages 230–246, 2018.
- [16] R. Horaud, F. Forbes, M. Yguel, G. Dewaele, and J. Zhang. Rigid and articulated point registration with expectation conditional maximization. *IEEE Transactions on Pattern Analysis and Machine Intelligence*, 33(3):587–602, 2010.
- [17] H. Jiang, J. Cai, and J. Zheng. Skeleton-aware 3d human shape reconstruction from point clouds. In *Proceedings of the IEEE/CVF International Conference on Computer Vision*, pages 5431–5441, 2019.
- [18] H. Joo, T. Simon, X. Li, H. Liu, L. Tan, L. Gui, S. Banerjee, T. Godisart, B. Nabbe, I. Matthews, et al. Panoptic studio: A massively multiview system for social interaction capture. *IEEE Transactions on Pattern Analysis and Machine Intelligence*, 41(1):190–204, 2017.
- [19] V. G. Kim, Y. Lipman, and T. Funkhouser. Blended intrinsic maps. *ACM transactions on graphics (TOG)*, 30(4):1–12, 2011.
- [20] N. Kolotouros, G. Pavlakos, M. J. Black, and K. Daniilidis. Learning to reconstruct 3d human pose and shape via model-fitting in the loop. In *Proceedings of the IEEE/CVF International Conference on Computer Vision*, pages 2252–2261, 2019.
- [21] C.-L. Li, T. Simon, J. Saragih, B. Póczos, and Y. Sheikh. Lbs autoencoder: Self-supervised fitting of articulated meshes to point clouds. In *Proceedings of the IEEE/CVF Conference on*

- Computer Vision and Pattern Recognition*, pages 11967–11976, 2019.
- [22] H. Li, R. W. Sumner, and M. Pauly. Global correspondence optimization for non-rigid registration of depth scans. In *Computer graphics forum*, volume 27, pages 1421–1430. Wiley Online Library, 2008.
 - [23] O. Litany, T. Remez, E. Rodola, A. Bronstein, and M. Bronstein. Deep functional maps: Structured prediction for dense shape correspondence. In *Proceedings of the IEEE International Conference on Computer Vision*, pages 5659–5667, 2017.
 - [24] M. Loper, N. Mahmood, and M. J. Black. Mosh: Motion and shape capture from sparse markers. *ACM Transactions on Graphics (ToG)*, 33(6):1–13, 2014.
 - [25] M. Loper, N. Mahmood, J. Romero, G. Pons-Moll, and M. J. Black. Smpl: A skinned multi-person linear model. *ACM Transactions on Graphics (ToG)*, 34(6):1–16, 2015.
 - [26] Q. Ma, J. Yang, A. Ranjan, S. Pujades, G. Pons-Moll, S. Tang, and M. J. Black. Learning to dress 3d people in generative clothing. In *Proceedings of the IEEE/CVF Conference on Computer Vision and Pattern Recognition*, pages 6469–6478, 2020.
 - [27] R. Marin, S. Melzi, E. Rodola, and U. Castellani. Farm: Functional automatic registration method for 3d human bodies. In *Computer Graphics Forum*, volume 39, pages 160–173. Wiley Online Library, 2020.
 - [28] A. Nguyen, M. Ben-Chen, K. Welnicka, Y. Ye, and L. Guibas. An optimization approach to improving collections of shape maps. 30(5):1481–1491, 2011.
 - [29] M. Ovsjanikov, M. Ben-Chen, J. Solomon, A. Butscher, and L. Guibas. Functional maps: a flexible representation of maps between shapes. *ACM Transactions on Graphics (TOG)*, 31(4):1–11, 2012.
 - [30] G. Pons-Moll, S. Pujades, S. Hu, and M. J. Black. Clothcap: Seamless 4d clothing capture and retargeting. *ACM Transactions on Graphics (ToG)*, 36(4):1–15, 2017.
 - [31] C. R. Qi, L. Yi, H. Su, and L. J. Guibas. Pointnet++: Deep hierarchical feature learning on point sets in a metric space. In *Advances in neural information processing systems*, pages 5099–5108, 2017.
 - [32] J. Romero, D. Tzionas, and M. J. Black. Embodied hands: Modeling and capturing hands and bodies together. *ACM Transactions on Graphics (ToG)*, 36(6):1–17, 2017.
 - [33] J.-M. Roufosse, A. Sharma, and M. Ovsjanikov. Unsupervised deep learning for structured shape matching. In *Proceedings of the IEEE/CVF International Conference on Computer Vision*, pages 1617–1627, 2019.
 - [34] J. Solomon, G. Peyré, V. G. Kim, and S. Sra. Entropic metric alignment for correspondence problems. *ACM Transactions on Graphics (ToG)*, 35(4):1–13, 2016.
 - [35] F. Tombari, S. Salti, and L. Di Stefano. Unique signatures of histograms for local surface description. In *European conference on computer vision*, pages 356–369. Springer, 2010.
 - [36] M. Vestner, R. Litman, E. Rodola, A. Bronstein, and D. Cremers. Product manifold filter: Non-rigid shape correspondence via kernel density estimation in the product space. In *Proceedings of the IEEE conference on computer vision and pattern recognition*, pages 3327–3336, 2017.
 - [37] C. Wan, T. Probst, L. V. Gool, and A. Yao. Self-supervised 3d hand pose estimation through training by fitting. In *Proceedings of the IEEE/CVF Conference on Computer Vision and Pattern Recognition*, pages 10853–10862, 2019.
 - [38] S. Wang, A. Geiger, and S. Tang. Locally aware piecewise transformation fields for 3d human mesh registration. In *Proceedings of the IEEE/CVF Conference on Computer Vision and Pattern Recognition*, pages 7639–7648, 2021.
 - [39] L. Wei, Q. Huang, D. Ceylan, E. Vouga, and H. Li. Dense human body correspondences using convolutional networks. In *Proceedings of the IEEE Conference on Computer Vision and Pattern Recognition*, pages 1544–1553, 2016.
 - [40] Q. Xu, W. Wang, D. Ceylan, R. Mech, and U. Neumann. Disn: Deep implicit surface network for high-quality single-view 3d reconstruction. In *Advances in neural information processing systems*, page 492–502, 2019.
 - [41] M. Ye and R. Yang. Real-time simultaneous pose and shape estimation for articulated objects using a single depth camera. In *Proceedings of the IEEE Conference on Computer Vision and Pattern Recognition*, pages 2345–2352, 2014.
 - [42] T. Yu, Z. Zheng, K. Guo, J. Zhao, Q. Dai, H. Li, G. Pons-Moll, and Y. Liu. Doublefusion: Real-time capture of human performances with inner body shapes from a single depth sensor. In *Proceedings of the IEEE conference on computer vision and pattern recognition*, pages 7287–7296, 2018.
 - [43] Y. Zhou, C. Barnes, J. Lu, J. Yang, and H. Li. On the continuity of rotation representations in neural networks. In *Proceedings of the IEEE/CVF Conference on Computer Vision and Pattern Recognition*, pages 5745–5753, 2019.